2015-08-14

The azimuthally averaged boundary layer structure of a numerically simulated major hurricane

Abarca, Sergio F.; Montgomery, Michael T.; McWilliams, James C.

AGU Publications

Abarca, S. F., M. T. Montgomery, and J. C. McWilliams (2015), The azimuthally averaged boundary layer structure of a numerically simulated major hurricane, J. Adv. Model. Earth Syst., 7, 12071219, doi:10.1002/ 2015MS000457

http://hdl.handle.net/10945/57131

AGU PUBLICATIONS

Journal of Advances in Modeling Earth Systems

RESEARCH ARTICLE

10.1002/2015MS000457

The azimuthally averaged boundary layer structure of a numerically simulated major hurricane

Sergio F. Abarca[1], Michael T. Montgomery[2], and James C. McWilliams[3]

[1]IMSG at NOAA/NWS/NCEP, College Park, Maryland, USA, [2]Naval Postgraduate School, Monterey, California, USA, [3]Institute of Geophysics and Planetary Physics, University of California, Los Angeles, Los Angeles, California, USA

Key Points:
- The hurricane's inner core boundary layer is found to be nonlinear
- There are departures from Ekman-like balance in the hurricane boundary layer
- Azimuthally averaged hurricane boundary layer lacks shock-like structures

Correspondence to:
S. F. Abarca,
sergio.abarca@noaa.gov

Citation:
Abarca, S. F., M. T. Montgomery, and J. C. McWilliams (2015), The azimuthally averaged boundary layer structure of a numerically simulated major hurricane, *J. Adv. Model. Earth Syst.*, *7*, 1207–1219, doi:10.1002/2015MS000457.

Received 19 MAR 2015
Accepted 18 JUL 2015
Accepted article online 23 JUL 2015
Published online 14 AUG 2015

Abstract This work examines the azimuthally averaged boundary layer structure of a numerically simulated hurricane. We nominally define the hurricane boundary layer as the layer in which the effects of surface friction are associated with significant departures from gradient wind balance. The boundary layer in the intensifying primary and forming secondary eyewalls is found to be nonlinear. At large radii, exterior to the eyewalls, Ekman-like balance as traditionally defined, is found to hold true. Where significant departures from Ekman-like balance are found, the departures are characterized by large vertical advection of horizontal velocity through the depth of the boundary layer. Shock-like structures are not found to be prominent in the azimuthally averaged view of the vortex boundary layer, with the largest azimuthally averaged radial gradients of the radial and tangential velocities being on the order of only a few meters per second per kilometer. Also, in the radial regions of the eyewalls, at the height where the averaged tangential wind is a maximum, the radial advection of radial velocity is an order of magnitude smaller than the agradient force per unit mass. Some physical implications of these findings are discussed.

1. Introduction

There is mounting evidence that the dynamics of the hurricane boundary layer is a key for understanding several aspects of tropical cyclone intensification and mature structure. For one thing, the boundary layer contributes to the radial distribution of moisture and convective instability via sea-to-air fluxes of latent and sensible heat and advective transport. For another, the boundary layer dynamics determines not only the absolute angular momentum of the air leaving the layer, but determines also where moist boundary layer air erupts out of the layer.

While different perspectives could be adopted to define the hurricane boundary layer [e.g., *Zhang et al.*, 2011], at an elementary level, the frictional boundary layer of a tropical cyclone arises on account of the frictional stress at the sea surface. In this work "friction" refers to the turbulent momentum flux divergence associated with the near-surface vertical shear and the surface drag stress at high Reynolds number. In comparison with the deep vortex flow aloft, the boundary layer is a relatively thin transition layer that connects the bulk vortex with the frictional surface.

Of course, there is some inherent fuzziness in providing a precise dynamical definition of the boundary layer top. The ambiguity arises in part because the frictional tendencies are likely to have different vertical structures in the different momentum equations and also because the agradient force (the departure from gradient wind balance) is not strictly zero above the boundary layer so defined. Despite such fuzziness, dynamical definitions of the hurricane boundary layer are uncontroversial in the outer regions of a hurricane, where convection is not prevalent and there is subsidence into the layer. However, dynamical definitions of the boundary layer are expected to have limitations in the inner-core region where boundary layer air is being lofted into the eyewall clouds. The flow in this region is akin to that of "separation" in aerodynamic boundary layers [e.g., *Anderson*, 2005] and conventional boundary layer theory formally breaks down here [*Smith and Montgomery*, 2010; *Montgomery et al.*, 2014a]. It is difficult to unambiguously define the top of the boundary layer in this region because significant departures from gradient wind balance are still present that are not directly associated with the surface drag.

In this study, we define nominally the hurricane boundary layer as the layer in which the effects of surface friction are associated with significant departures from gradient wind balance. More specifically, we follow

common practice by defining the boundary layer top as the height at which either the departure from gradient wind balance vanishes or the magnitude of friction asymptotically approaches a constant (sometimes zero).

Despite the widely acknowledged importance of the boundary layer, there are differing views on the *dynamical role* of the boundary layer in the spin-up and mature structure of a tropical cyclone vortex. A survey of the scientific literature reveals an eclectic mix of ideas being debated currently. For example, in an effort to explain the unprecedented flight-level observations along a radial flight track at approximately 500 m altitude in the rapidly intensifying Hurricane Hugo [*Marks et al*., 2008], some research has proposed that "shock-like" structures—akin to the classical Burgers equation [e.g., *Whitham*, 1974]—are essential elements in the boundary layer dynamics of the inner core of an intensifying and mature tropical cyclone [*Williams et al*., 2013; *Williams*, 2015; *Slocum et al*., 2014]. Other work argues that a quasi-linear generalization of Ekman theory suffices for obtaining a zero-order understanding of the role of the boundary layer in the dynamics of secondary eyewall formation [*Kepert*, 2013].

Still other work argues that the boundary layer dynamics of the rapidly rotating region of a tropical cyclone are intrinsically nonlinear [e.g., *Smith*, 1968; *McWilliams*, 1971; *Smith and Montgomery*, 2010; *Montgomery et al*., 2014b] and cannot be captured consistently by axisymmetric balance theory [e.g., *Bui et al*., 2009; *Abarca and Montgomery*, 2013, 2014] or quasi-linear Ekman theory. In this nonlinear view, the boundary layer takes on a new dynamical role during vortex intensification in association with the convergence of absolute angular momentum (M). Although M is not materially conserved in the boundary layer, large tangential wind speeds can be achieved there if the radial inflow is sufficiently large to bring the air parcels to small radii with minimal loss of M. This spin-up mechanism, while coupled to the interior flow dynamics via the radial pressure gradient at the top of the boundary layer, is tied fundamentally to the dynamics of the boundary layer, where the flow is not in gradient wind balance over a substantial radial span. Indeed, it has been shown using theoretical analyses and observational data that this boundary layer spin-up mechanism accounts for the occurrence of the maximum tangential wind in the boundary layer [*Bui et al*., 2009; *Sanger et al*., 2014; *Montgomery et al*., 2014a], a feature that has been found also in prior observational studies [*Montgomery et al*., 2006b; *Kepert*, 2006; *Bell and Montgomery*, 2008; *Zhang et al*., 2011].

The differing views of the boundary layer summarized above motivate basic science questions about the nature of the dynamics of the hurricane boundary layer. For example, what is the most suitable way to think about the dynamics of the hurricane boundary layer? Is the azimuthally averaged boundary layer structure of a hurricane vortex adequately described by Ekman-like dynamics, or shock-like dynamics? The aim of this paper is to contribute toward answering these questions using a reasonably high-resolution "full-physics" mesoscale simulation of a mature hurricane vortex.

An outline of the remainder of the paper is as follows. Section 2 reviews the physics of Ekman-type balance in tropical cyclone vortices. Section 3 introduces our methodology to investigate the dynamical structure of the hurricane boundary layer. Section 4 presents and discusses the results. Section 5 offers our conclusions and recommendations.

2. Ekman-Type Models for Hurricane-Like Vortices Revisited

As described by *Gill* [1982], *Holton* [2004], and *McWilliams* [2011], the classical Ekman balance comprises a balance between three horizontal forces: Coriolis, pressure gradient, and friction. The boundary layer flow is characterized by a large Reynolds number and is therefore turbulent. By friction, then, we mean the divergence of the Reynolds-averaged eddy momentum flux caused by the surface stress. According to the boundary layer approximation, this frictional force per unit mass may be approximated by the vertical divergence of the mean vertical flux of horizontal eddy momentum. Assuming horizontal homogeneity and assuming a K-theory turbulence closure to parameterize the turbulence effects, the horizontal force balance is expressed in Cartesian coordinates as follows:

$$-fv = -\frac{1}{\rho}\frac{\partial p}{\partial x} + \frac{\partial}{\partial z}\left(K\frac{\partial u}{\partial z}\right)$$

$$fu = -\frac{1}{\rho}\frac{\partial p}{\partial y} + \frac{\partial}{\partial z}\left(K\frac{\partial v}{\partial z}\right)$$

where the indicated variables have their usual meaning and K is a vertically variable momentum diffusivity.

For curvilinear flows, such as a rapidly rotating vortex overlying a solid frictional surface or ocean, (nonlinear) Ekman-type models may be postulated by relaxing the horizontal homogeneity assumption and including versions of the apparent forces that arise from the circular geometry of the flow. In a cylindrical polar coordinate system for a stationary axisymmetric vortex, an Ekman-type model can be formulated as follows. Let $\bar{V}$ denotes the azimuthally averaged swirling tangential velocity at the top of the boundary layer, assumed to be in gradient wind balance with the azimuthally averaged pressure field $\bar{P}$:

$$f\bar{V} + \frac{\bar{V}^2}{r} = \frac{1}{\bar{\rho}}\frac{\partial \bar{P}}{\partial r}$$

where $\bar{\rho}$ is the azimuthal average density of moist air and r is radius from the center of circulation. Now let v denotes the departure of the total tangential velocity from the averaged gradient wind velocity and let the radial velocity in the boundary layer be denoted as u. Then, for small departures from this gradient balance configuration, the first-order boundary layer momentum balance in the radial direction is between the residual cyclogeostrophic force and radial friction:

$$-v\left(f + \frac{2\bar{V}}{r}\right) = \frac{\partial}{\partial z}\left(K\frac{\partial u}{\partial z}\right)$$

In this view, departures from gradient wind balance (left-hand side) are balanced by the vertical gradient of the Reynolds-averaged shear stress in the radial direction (right-hand side). To connect this simplified momentum balance with upcoming language used in section 3, we will refer to the negative of the left-hand side of this equation as the "Ekman Agradient Force," defined as:

$$AF_{Ek} = v\left(f + \frac{2\bar{V}}{r}\right)$$

In the tangential direction, the first-order momentum balance is between the radial flux of mean absolute vorticity and the vertical gradient of the Reynold-averaged stress:

$$u\left(f + \frac{\bar{V}}{r} + \frac{\partial \bar{V}}{\partial r}\right) = \frac{\partial}{\partial z}\left(K\frac{\partial v}{\partial z}\right)$$

The foregoing Ekman-type model has been used frequently in the hurricane literature because it appears to capture in some respects certain structural features of the hurricane boundary layer flow. These features include the radial distribution of the vertical velocity at the top of the boundary layer [e.g., *Eliassen*, 1971; *Eliassen and Lystad*, 1977] and the existence of the tangential wind maximum within the boundary layer [*Kepert*, 2001; *Kepert and Wang*, 2001]. This Ekman-type model is still being used as a theoretical framework for understanding the key role of the boundary layer in, for example, secondary eyewall formation and evolution [*Kepert*, 2013; *Kepert and Nolan*, 2014].

For a steady state boundary layer flow, the foregoing system neglects the nonlinear advection of radial velocity as well as the radial and vertical advection of perturbation tangential velocity. If we extend our boundary layer to include the viscous sublayer where the air velocity must match that of the relatively small (effectively zero) ocean current velocity, we note here that because v must be of the size of $\bar{V}$ to satisfy the surface boundary condition, and u is comparable to v because of the expected Ekman layer spiral, there is a leading-order inconsistency by including the linear advective fluxes ($u\bar{V}$, $v\bar{V}$) while neglecting the nonlinear ones (uu, uv, vv). This reasoning is complimentary to the scale analysis and the calculations presented in *Vogl and Smith* [2009] for a semislip lower boundary condition for the eddy stress at anemometer level that is more widely used in geophysical vortex dynamics [e.g., *Eliassen*, 1971; *Rotunno and Emanuel*, 1987]. Indeed, we will see below that some of these nonlinear horizontal advective terms are often significant over a relatively sizeable depth of the boundary layer momentum balance, as are the vertical ones (uw, vw).

3. Analysis Methodology

The methodology of this work consists of examining the kinematics and dynamics (through the radial and tangential momentum budgets) in a mature storm, simulated with the Regional Atmospheric Modeling System (RAMS) [*Pielke et al*., 1992; *Cotton et al*., 2003]. The analyzed storm was originally introduced by *Terwey and Montgomery* [2008] and was revisited by *Terwey et al*. [2013], *Abarca and Montgomery* [2013, 2014], and *Montgomery et al*. [2014b]. A full description of the simulation and its evolution is presented by *Terwey and Montgomery* [2008]. Here we highlight that the simulation uses a surface flux parameterization based on the *Louis* [1979] scheme (a scheme recommend by *Kepert* [2012]); the radiation scheme introduced by *Harrington* [1997]; a subgrid scale turbulence scheme based on *Smagorinsky* [1963], with the modifications from *Lilly* [1962] and *Hill* [1974]; and the seven-species microphysical scheme by *Walko et al*. [1995], with the specification described in *Montgomery et al*. [2006a]. While we focus our analysis here on the presented RAMS integration, all the conclusions of this study are found to be consistent with recent diagnoses by the first author using a realistic integration of Hurricane Igor (2010). The Igor simulation was performed by *Davis et al*. [2008] using the Advanced Research core of the Weather Research and Forecasting (AHW) model. The simulation was produced by The Hurricane Group in the Mesoscale and Microscale Meteorology Division of the National Center for Atmospheric Research (NCAR) and will be described in detail in an upcoming publication.

The RAMS simulation is an idealized integration on an *f*-plane (15°N), with sea surface temperature held constant (28°C). It is executed in three domains, with the two nested domains featuring two-way interactions. The nested domains are located at the center of the corresponding parent domain. The domains sizes are 168, 170, and 251 grid points with grid spacing of 24, 6, and 2 km, for the largest, middle, and smallest domains, respectively. The integration is performed with 30 vertical levels (with vertical grid spacing varying from 300 m near the surface to 1.8 km, at about 26 km altitude). The initial condition is characterized by a quiescent environment (*Jordan*'s [1958] sounding); a weak mesoscale cyclonic vortex (10 m s^{-1} maximum tangential wind speed at 4 km height and 75 km radius) at the center of the three domains. The initial vortex is assumed to be in thermal wind balance and possesses a positive axisymmetric moisture anomaly near the center (water vapor mixing ratio anomaly gradually increased to 1.3 g kg^{-1} at vortex center).

The simulation is integrated for 216 h. Following *Terwey and Montgomery* [2008] and *Abarca and Montgomery* [2013], hour 156 is relabeled as hour 0. Further details of the RAMS experimental setup and prior analyses can be found in the collection of papers by *Terwey and Montgomery* [2008], *Montgomery et al*. [2006a], *Terwey et al*. [2013], and *Abarca and Montgomery* [2013].

To optimally analyze the nearly axisymmetric vortex, we remap the RAMS variables from their original representation in a Cartesian coordinate system into a cylindrical polar coordinate system. The center of the coordinate system is chosen to be the location where the differences between the azimuthally averaged radially profiles of sea level pressure and individual profiles taken to the north, south, east, and west were minimized following the methodology of *Cram et al*. [2007]. We note that the results exhibit negligible differences when computed with the center obtained as the centroid of the potential vorticity field in the lowest 7.3 km of the domain (not shown). The vertical grid spacing of the cylindrical grid is the same as with the Cartesian grid. The radial and azimuthal grid spacing are 2 km and 1 degree of azimuth, respectively.

The radial and tangential momentum tendency equations are analyzed in their respective material forms using a traditional "azimuthal mean flow" plus "azimuthal eddy" partitioning as follows:

$$\frac{\partial \bar{u}}{\partial t}+\bar{u}\frac{\partial \bar{u}}{\partial r}+\bar{w}\frac{\partial \bar{u}}{\partial z}+\overline{u'\frac{\partial u'}{\partial r}}+\overline{\frac{v'}{r}\frac{\partial u'}{\partial \lambda}}+\overline{w'\frac{\partial u'}{\partial z}}=\frac{\bar{v}^2}{r}+\overline{\frac{v'^2}{r}}+f\bar{v}-\frac{1}{\bar{\rho}}\frac{\partial \bar{p}}{\partial r}-\overline{\frac{1}{\rho}\frac{\partial p'}{\partial r}}+F_r \tag{1}$$

$$\frac{\partial \bar{v}}{\partial t}+\bar{u}\frac{\partial \bar{v}}{\partial r}+\bar{w}\frac{\partial \bar{v}}{\partial z}+\overline{u'\frac{\partial v'}{\partial r}}+\overline{w'\frac{\partial v'}{\partial z}}=-\frac{\bar{u}\bar{v}}{r}-\overline{\frac{u'v'}{r}}-\overline{\frac{1}{r\rho}\frac{\partial p'}{\partial \lambda}}-f\bar{u}+F_\lambda \tag{2}$$

Here (u, v, w) are the radial, tangential, and vertical wind velocities; r, λ, and z are the radial, tangential, and vertical coordinates; t is time, ρ is air density, p is pressure, and F_u and F_v are the radial and tangential components of the radial and tangential momentum subgrid scale eddy flux divergence, computed as a residual from equations (1) and (2). As is usual in this type of flow partitioning, overbars represent azimuthal averages on constant height surfaces and the primes denote perturbation (eddy) values, computed as

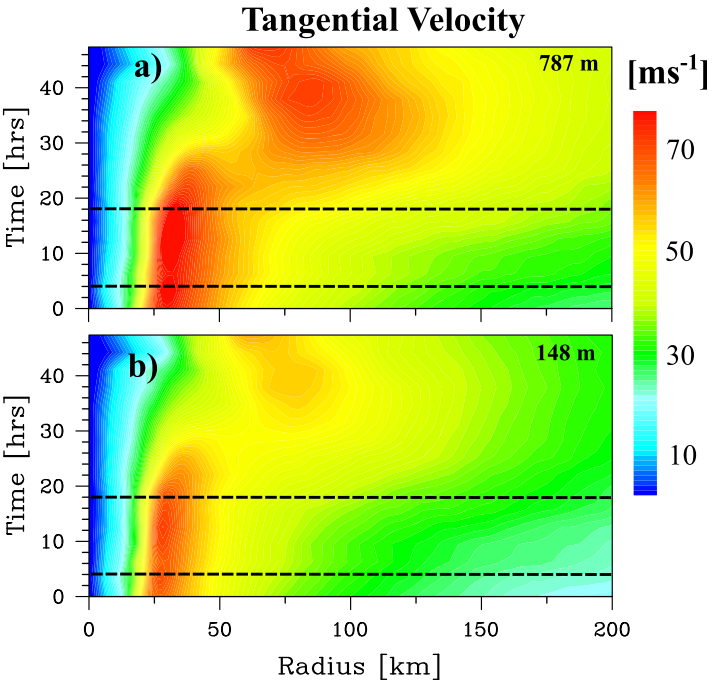

Figure 1. Radius-time plot of the RAMS azimuthally averaged tangential velocity (m s^{-1}) at 148 and 787 m height. The dashed black lines indicate hour 4 and hour 18, where the rest of the study focuses.

departures from the azimuthal averages. (The same caveat expressed by *Persing et al*. [2013] concerning the physical meaning of the "mean" and "eddy" terms for highly localized structures in azimuth—e.g., with vortical hot towers—applies here as well.) The terms of equations (1) and (2) are computed from instantaneous fields (A comparison of the results using 1 and 2 h averages, based on 6 min frequency output—not shown—, indicates that the differences are negligible in the context of the conclusions of this study.), except for the time tendencies, which are obtained as 6 h integrals of centered time differences (using 6 min output). As noted above, the frictional tendency terms are computed via residual. As an example, the tangential subgrid tendency term in equation (2) is obtained as the difference between the sum of the local time change of tangential momentum, mean absolute vorticity flux, the mean vertical advection, the corresponding eddy terms and the apparent forces and azimuthal pressure gradient.

In this fully nonlinear context, in the radial momentum equation, departures from gradient wind balance associated with the reduction of the tangential velocity component by tangential friction are accompanied by an effective force that generally does not balance the radial friction force. The specific force is called here the *agradient force* and is defined following *Smith et al*. [2009] as:

$$AF = -\frac{1}{\bar{\rho}}\frac{\partial \bar{p}}{\partial r} + \frac{\bar{v}^2}{r} + f\bar{v} \tag{3}$$

In the subsequent analysis, we will confine our attention to the lowest 3 km of the inner core of the vortex, particularly the intensifying primary eyewall, the forming secondary eyewall, and a region radially outside the forming secondary eyewall.

4. Results

4.1. Boundary Layer Kinematics

Figure 1 shows the radius-time diagrams of the azimuthal mean tangential velocity at the heights of 148 and 787 m. It is similar to Figure 2 in *Terwey et al*. [2013] and Figure 1 in *Abarca and Montgomery* [2013, 2014]. The figure summarizes the canonical eyewall replacement cycle of the simulation. From the azimuthally averaged perspective, the primary eyewall is intensifying up to hour 15 after which time its azimuthally averaged tangential winds weaken monotonically. Radially outside of the primary eyewall, there is a progressive amplification of the azimuthally averaged tangential winds that extend beyond the domain shown (200 km). From about hour 24, in the radial region of the tangential velocity amplification, the secondary wind maximum of the secondary eyewall emerges. Finally, the figure shows the radial contraction of the secondary wind maximum that completes eyewall replacement cycle. In this study, we focus on hours 4 and 18, when the primary eyewall was intensifying and when the secondary eyewall was forming, respectively.

Figure 2 shows the radial profiles of the azimuthally averaged radial, tangential, and vertical velocity components, within the boundary layer of the storm's inner core at four vertical levels between 148 and 1138 m

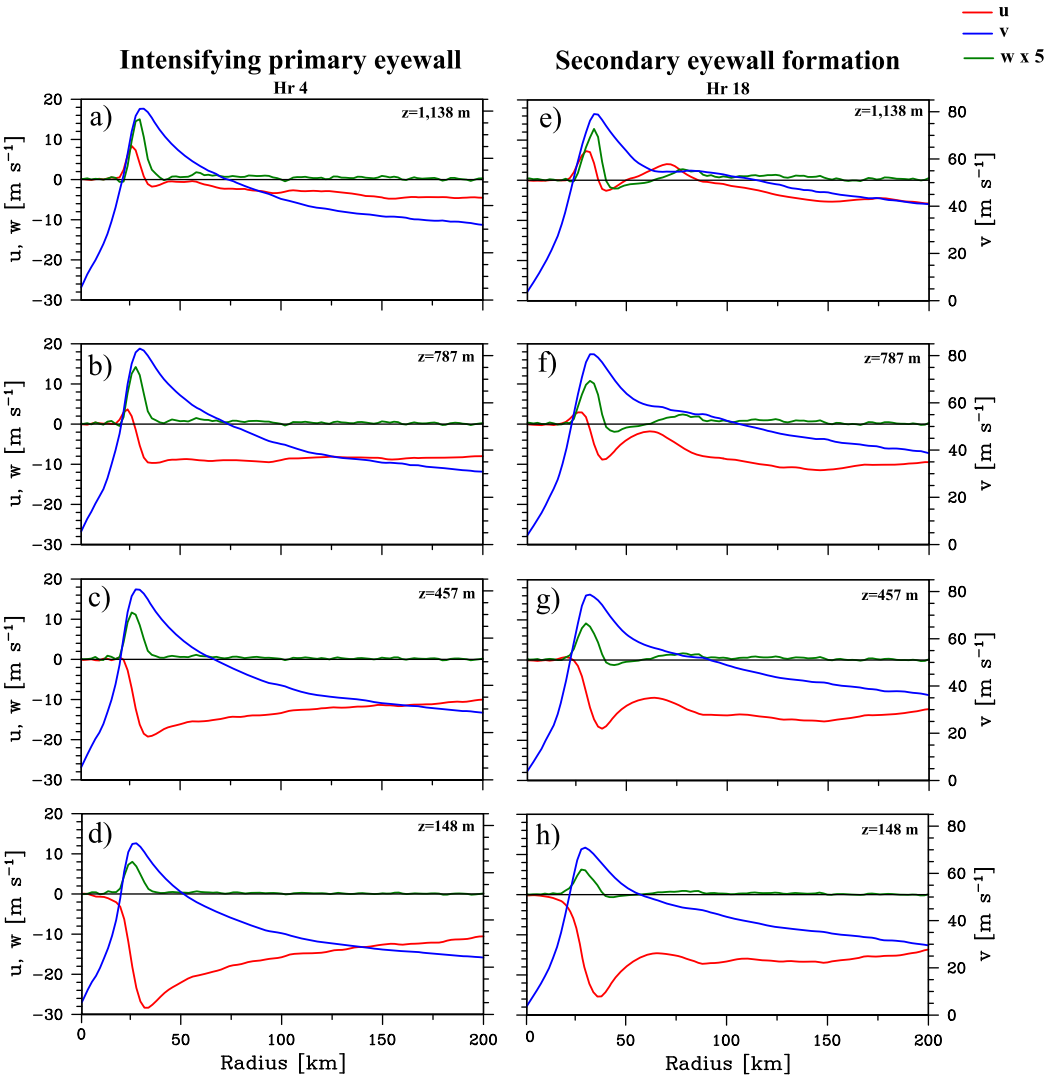

Figure 2. Azimuthally averaged tangential (blue), radial (red), and vertical (green) velocity components (m s^{-1}), as a function of radius, at (left) hour 4 and (right) hour 18 at the heights of (top row) 1138 m, (second row) 787 m, (third row) 457 m, and (bottom row) 148 m. For display clarity, the average vertical velocity component is multiplied by a factor of 5.

height. The times chosen correspond to the intensification of the primary eyewall (hour 4) and during secondary eyewall formation (hour 18). These times have been found to be representative of the intensification of the primary eyewall and the formation of the secondary eyewall within the first 20 h depicted in Figure 1.

From Figure 2, we see that the largest value (and radial gradients) of the radial velocity occurs at 148 m height (the lowest level considered), while the largest tangential velocity occurs at 787 m height. The largest vertical velocity occurs at the highest level shown (1138 m). Such a distribution of the maxima of the velocity components is found to hold true for the intensifying primary eyewall (hour 4, left plots) and the forming secondary eyewall (hour 18, right plots). The vertical location of the maximum values of the horizontal wind components is consistent with the general understanding of the horizontal momentum balances: the strong inflow velocity is primarily attributable to the effects of friction and it reaches its maximum magnitude at the lowest levels, where vertical momentum diffusion and the agradient force are the largest. The tangential velocity reaches its maximum near the top of the frictional boundary layer, where the radial advection of tangential momentum surpasses its depletion. The vertical structure of the horizontal momentum budgets is discussed below.

Throughout the boundary layer, the largest azimuthally averaged radial gradients in radial and tangential velocity occur in the primary eyewall, both during the intensification of the primary eyewall (hour 4, Figure 2, left plots) and during secondary eyewall formation (hour 18, Figure 2, right plots). The largest azimuthally

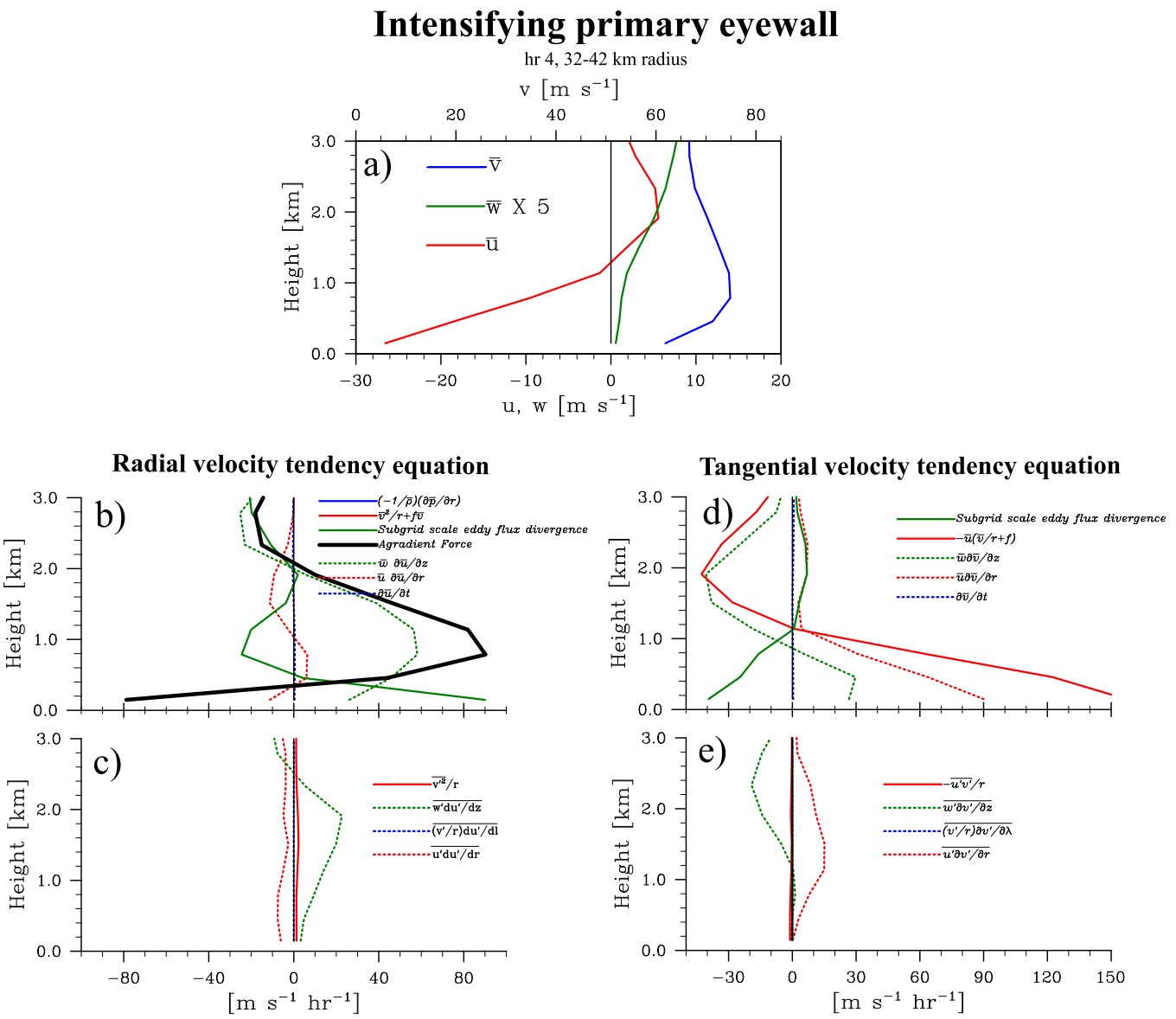

Figure 3. Vertical profiles of (a) the three velocity components and (b–e) the radial and tangential velocity tendency equations at hour 4. The quantities presented correspond to 10 km radial averages radially outward of the radius of maximum winds (32–42 km radius). In the momentum budgets, the dotted lines correspond to the components of the material derivative and are plotted as positive on the left-hand side of equations (1) and (2), the solid lines correspond to the different forces in the budget and are plotted as positive on the right-hand side of equations (1) and (2). See text for details.

averaged radial gradients in Figure 2 have values on the order of 2 m s^{-1} km^{-1} and those during secondary eyewall formation are at least an order of magnitude smaller. Such values are in contrast to the local radial change of about 60 m s^{-1} in about 1 km highlighted by *Williams et al.* [2013], as they were observed in Hurricane Hugo (1989). Although smaller magnitudes of the radial gradients are expected in an azimuthally averaged view than those obtained from in situ observations along a radial flight segment through the eyewall, the smallness of the azimuthally averaged radial gradients in the radial region of secondary eyewall formation (and even during the radial contraction of the mature secondary eyewall that are about 1 m s^{-1} km^{-1}, not shown) does not support the idea that shock-like structures are relevant in the azimuthally averaged view of secondary eyewall formation and evolution [cf. *Williams et al.*, 2013; *Williams*, 2015; *Slocum et al.*, 2014].

4.2. Boundary Layer Dynamics

Figures 3–5 show the vertical structure of the three velocity components as well as the vertical structure of the terms in equations (1)–(3) during the primary eyewall intensification (Figure 3) and during the formation

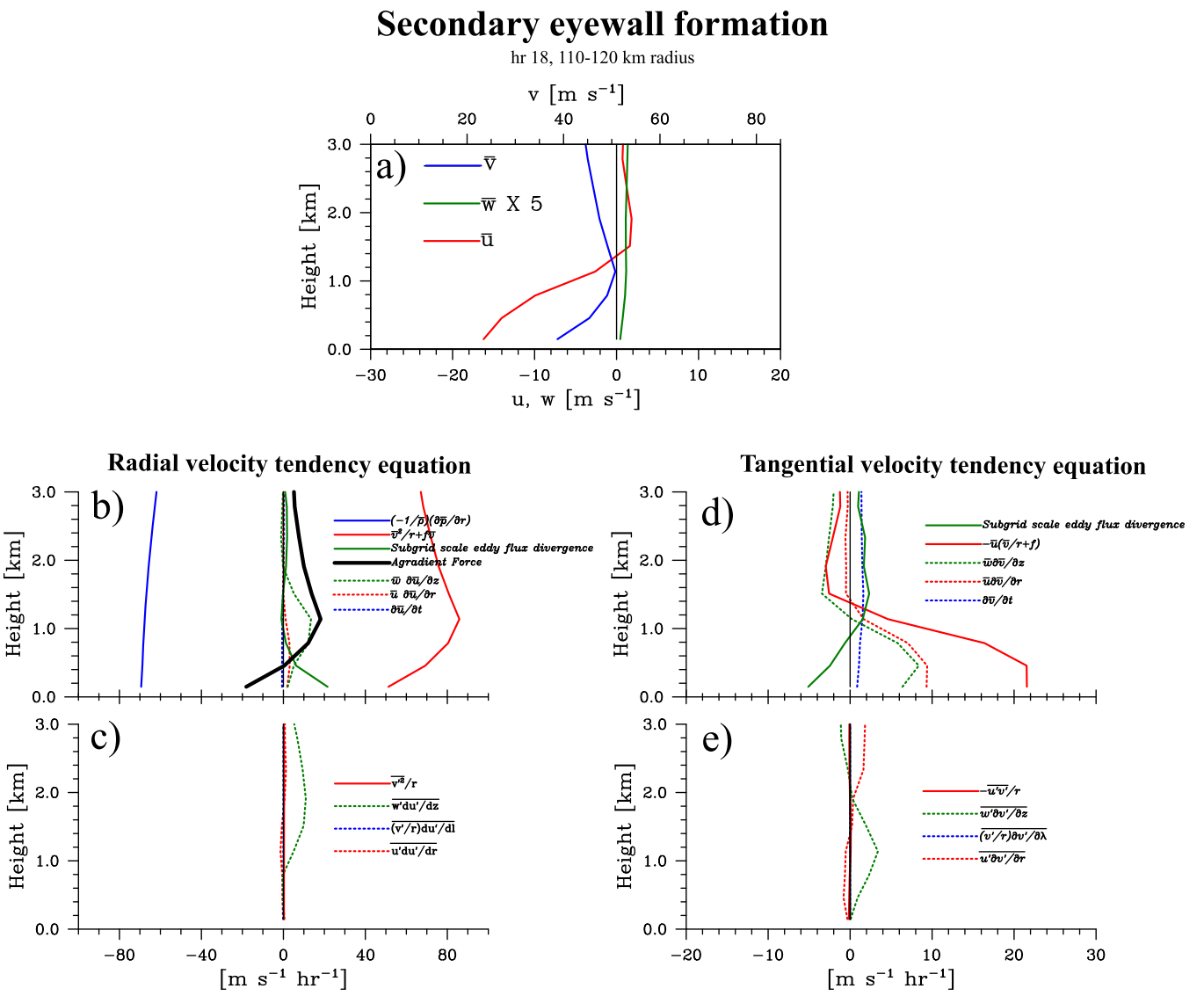

Figure 4. As Figure 3, but for hour 18 and the quantities correspond to 10 km radial averages in the region of largest tangential wind tendency during secondary eyewall formation (110–120 km radius). See text for details.

of the secondary eyewall (Figures 4 and 5). The terms involving perturbation pressure are not shown (they were found negligible compared to the rest of the terms and would appear as vertical lines at the zero value in the presented diagrams). Figures 3–5 show 10 km radial averages and their results are consistent with those obtained using single radius and 5, 15, and 20 km radial averages (not shown). For convenience of presentation, Figure 3 shows radial averages between 32 and 42 km. This averaging interval is 10 km radially outward from the radius of maximum winds and is chosen to highlight the processes leading to the emergence of the maximum tangential wind in the storm. Figure 4 presents radial averages taken between 110 and 120 km radius, focusing on the region with the largest spin-up tendency associated during the formation of the secondary eyewall [see *Abarca and Montgomery*, 2014, Figure 5j]. Finally, in order to include a representative picture of the storm's dynamical boundary layer structure outside the strongly convective region of the vortex, Figure 5 shows radial averages taken between 190 and 200 km radius. In the subsequent discussion, we refer to the radial region of Figure 3 as *the intensifying primary eyewall region*, to the radial region of Figure 4 as *the secondary eyewall formation region*, and to the radial region of Figure 5 as *the region at large radii*, respectively.

Figures 3a, 4a, and 5a highlight similarities and differences in the velocity field in the boundary layer dynamical structure between the intensifying primary eyewall, the secondary eyewall formation region, and

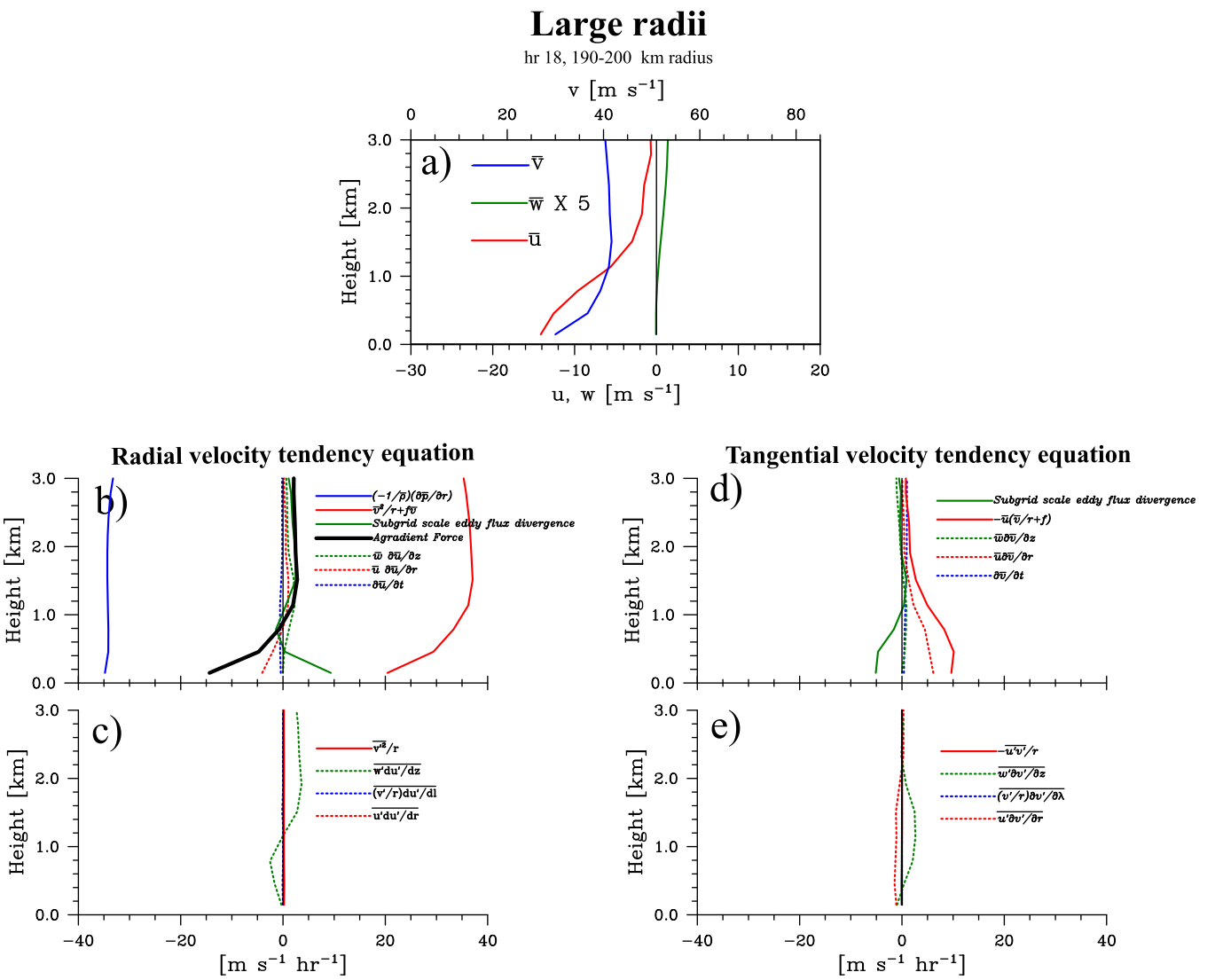

Figure 5. As Figures 3 and 4, but for hour 18 and the quantities correspond to 10 km radial averages in a region within the inner core but radially outside of the eyewalls (190–200 km radius). See text for details.

the region at large radii. As proposed in section 1, the boundary layer top can be nominally defined as the height where the disruption of gradient wind balance associated with the effects of surface friction vanishes. According to this definition, the boundary layer top is seen to reside at a height of about 2.0 km in the intensifying primary eyewall (Figure 3b), at about 2.5 km in the secondary eyewall formation region (Figure 4b), and close to 1.0 km in the region at large radii (Figure 5b). An alternative way to define the boundary layer top is the height at which friction asymptotically approaches a constant (sometimes zero), inclusive of both radial and tangential momentum balances. This second definition gives a boundary layer height of about 2.5–3, 1.6, and 1.0 km height for the intensifying primary eyewall, the forming secondary eyewall, and large radii, respectively. The two definitions of the dynamical boundary layer heights are broadly consistent with each other.

In the radial regions of the intensifying primary eyewall and forming secondary eyewall, the tangential velocity attains its maximum at $z \sim 787$ m and $\sim$1.1 km height, respectively. Based on the foregoing diagnoses of the boundary layer top, it is clear that the tangential velocity maximum occurs within the boundary layer (Figures 3a and 4a). In contrast, in the radial region of large radii the height of the tangential velocity maximum ($\sim$1.5 km, Figure 5a) is marginally higher than the top of the boundary layer ($\sim$1.0 km according to either definition considered). As the radius increases, the tangential velocity maximum is also less

pronounced relative to its nearby vertical value in the bulk vortex. From Figures 3a, 4a, and 5a, the difference in magnitude of the tangential velocity between the local maximum and the value found at 3 km height is 8, 6, and 2 m s^{-1}, respectively.

In the three radial regions highlighted here, the radial velocity is characterized by a layer of relatively strong inflow in the lowest levels. This inflow reaches its largest value at the lowest level shown (148 m). The regions of the intensifying primary eyewall and secondary eyewall formation contain a layer of outflow immediately surmounting the layer of strong inflow. Such an outflow layer is more pronounced in the intensifying primary eyewall region (outflow velocity of 6 m s^{-1}) than in the region of the forming secondary eyewall (outflow velocity of 2 m s^{-1}). A corresponding outflow layer at large radii is not present at all. In the three regions, the vertical velocity increases with height, up to a value of $\sim$2 m s^{-1} in Figure 3a, $\sim$0.4 m s^{-1} in Figure 4a, and $\sim$0.3 m s^{-1} in Figure 5a.

Ekman-like balance is found at large radii (Figures 5b–5e). In the radial momentum equation (Figures 5b and 5c), there is an approximate balance between the subgrid scale eddy flux divergence of radial momentum and the inward directed agradient force, i.e., the Ekman Agradient Force as defined in section 2. In the tangential momentum equation (Figures 5d and 5e), there is an approximate balance between the subgrid scale eddy flux divergence of tangential momentum and the radial flux of mean absolute vertical vorticity (which is the result of adding the centrifugal and the Coriolis forces and the radial advection of tangential momentum multiplied by -1). In this radial region, the mean and eddy components of the radial and vertical advection of radial momentum, as well as the mean and eddy components of the vertical advection of tangential momentum, are relatively small. Thus, an Ekman-like balance, like the one originally proposed by *Eliassen* [1971], is found here.

Unlike the large radii radial region, Ekman-like balance is not found in the regions of the intensifying primary eyewall or the forming secondary eyewall. In both of these regions, the subgrid scale eddy flux divergence of radial momentum in the radial momentum equation (Figures 3b and 4b) is too small to balance the agradient force throughout the depth of the boundary layer. The departures from Ekman-like balance are particularly large at the heights where the agradient force is directed radially outward. The tangential velocity is supergradient here [*Sanger et al*., 2014; *Smith et al*., 2009] and the maximum tangential velocity is found in this region.

Similarly, in the tangential momentum equation (Figures 3d and 4d), the subgrid scale eddy flux divergence of tangential momentum is too small to balance the radial flux of mean absolute vorticity through the depth of the boundary layer. Such significant departures from Ekman-like balance found in the intensifying primary eyewall and the forming secondary eyewall are characterized by large mean vertical advection of mean horizontal velocity through the depth of the boundary layer (Figures 3b, 3d, 4b, and 4d).

Our finding of the dynamical importance of the aforementioned nonlinear acceleration terms is consistent with the scale analysis, calculations and physical interpretation provided by *Vogl and Smith* [2009]. These findings do not support the hypothesis that the dynamics of the boundary layer in the eyewalls of a mature storm is adequately captured by Ekman-like theory [*Kepert*, 2013; cf. *Montgomery et al*., 2014a].

Another point to examine here concerns the structure of the mean radial advection comprising part of the radial acceleration near the height of tangential wind maximum. In the radial regions of the eyewalls, at the height where the tangential wind is a maximum (see Figures 3a and 4a), the mean radial advection of mean radial velocity is an order of magnitude smaller than the agradient force (Figures 3b and 4b). This finding does not support the idea that the mean radial advection of mean radial velocity, and corresponding "shock-like" structures, are essentially related to the generation of supergradient winds in the boundary layer.

There is one additional and noteworthy finding that emerges in our analysis of the azimuthal mean boundary layer structure of a mesoscale simulation of a mature hurricane vortex. For the three radial regions considered, the radial subgrid scale force exceeds that of the corresponding tangential subgrid scale force near the lower surface. In retrospect, this is perhaps not surprising given the large vertical shear of the inflow velocity near the lower surface in comparison to the corresponding vertical shear of the tangential velocity. However, it would certainly be incorrect to omit the radial subgrid scale force in favor of the tangential subgrid scale force in theoretical attempts to analyze the boundary layer dynamics of a hurricane vortex

[cf. *Stern et al*., 2015]. The full implication of the finding that the radial frictional force is comparable to or larger than the tangential frictional force near the lower surface awaits further analysis.

In closing the results section of this paper, we reiterate that while we focus our analysis here on the presented RAMS integration, all the conclusions of this study are found to hold true in an analogous analysis based on a realistic WRF integration of Hurricane Igor (2010) having a lowest model level of 50 m. This companion analysis will be presented in due course.

5. Conclusions

In this paper, we have examined the azimuthally averaged boundary layer structure of a numerically simulated hurricane that underwent secondary eyewall formation. This analysis aims toward a clarification on the dynamical nature of the hurricane boundary layer. Examples of contrasting views on the dynamical role of the boundary layer are: "Shock-like" structures—akin to the classical Burgers equation; quasi-linear generalizations of Ekman theory; and a fully nonlinear conception. This study focuses on three key radial regions of the boundary layer of the simulated mature hurricane: the intensifying primary eyewall, the forming secondary eyewall, and large radii (considered at about 200 km radius).

We defined nominally the hurricane boundary layer as the layer in which the effects of surface friction are associated with significant departures from axisymmetric gradient wind balance. We specifically considered two plausible definitions for the boundary layer top. The first definition is the height at which the departure from gradient wind balance vanishes. The second definition is the height at which the magnitude of horizontal friction asymptotically approaches a constant (sometimes zero). These dynamical definitions were found to give comparable boundary layer heights. The azimuthally averaged tangential wind maximum was found to be located well within the boundary layer of both primary and secondary eyewalls and found to be located marginally above the boundary layer at large radii. In all radial regions considered, the maximum radial velocity is located at the lowest level considered. These modeling results are consistent with the observational findings of *Kepert* [2006], *Montgomery et al*. [2006b], *Sanger et al*. [2014], and *Montgomery et al*. [2014b].

Although Ekman-like balance is found at large radii, it is not found in the regions of the intensifying primary eyewall and the forming secondary eyewall. At large radii, there is an approximate balance between the subgrid scale eddy flux divergence of horizontal momentum and the inward directed agradient force in the radial momentum equation, and the radial flux of mean absolute vorticity in the tangential momentum equation. In the regions of the intensifying primary eyewall and the forming secondary eyewall, Ekman-like balance is not found. In these radial regions, the subgrid scale eddy flux divergence of horizontal momentum is too small to balance, respectively, the agradient force in the radial momentum equation, and the radial flux of mean absolute vorticity in the tangential momentum equation. Significant departures from Ekman-like balance are characterized primarily by large mean vertical advection of mean horizontal velocity through the depth of the boundary layer. The dynamical importance of these nonlinear terms is consistent with the scale analysis, calculations, and physical interpretation provided by *Vogl and Smith* [2009] who conducted a test of the validity of the Ekman-like model using analytical solutions for the quasi-linear Ekman layer. In the full physics simulation examined here, eddy advection terms contribute also to the departures from Ekman-like balance, albeit to a lesser degree than the mean advection terms (that have larger magnitude).

Shock-like structures are not found to be prominent in the azimuthally averaged view of the hurricane's boundary layer. The largest azimuthally averaged radial gradients in radial and tangential velocity occur in the primary eyewall, and are about 2 m s^{-1} km^{-1}. Also, in the radial regions of the eyewalls, at the height where the tangential wind is a maximum, the mean radial advection of mean radial velocity is an order of magnitude smaller than the agradient force per unit mass.

Additionally, we documented that near the lower surface, the radial subgrid scale force exceeds that of the corresponding tangential subgrid scale force. The findings of the present study highlight the intrinsically nonlinear nature of the boundary layer in the simulated hurricane. The findings do not support the proposed ideas that the fluid dynamics of the boundary layer in the eyewalls of the storm are adequately captured by Ekman-like theory or that shock-like structures are relevant in the azimuthally averaged view of

secondary eyewall formation. Finally, we noted that while we focus our analysis on the presented RAMS integration, all the conclusions of this study are consistent with those from an analogous analysis based on a realistic WRF integration of hurricane Igor (2010). Such a companion analysis will be presented in due course.

Acknowledgments
This work was supported in part by National Science Foundation Awards AGS 0733380 and IAA-1313948. We thank Roger Smith for providing useful comments on a near-final draft of this paper. Sergio F. Abarca gratefully acknowledges the support from the National Research Council (NRC) through its Research Associateship Program, and the host institution, the Naval Postgraduate School (NPS) in Monterey, California. The views expressed herein are those of the authors and do not represent sponsoring agencies or institutions. The data used in this paper can be accessed by emailing the first author at sergio.abarca@noaa.gov.

References

Abarca, S. F., and M. T. Montgomery (2013), Essential dynamics of secondary eyewall formation, *J. Atmos. Sci.*, *70*, 3216–3230.
Abarca, S. F., and M. T. Montgomery (2014), Departures from axisymmetric balance dynamics during secondary eyewall formation, *J. Atmos. Sci.*, *71*, 3723–3738.
Anderson, J. D. (2005), Ludwig Prandtl's boundary layer, *Phys. Today*, *58*, 42–48.
Bell, M. M., and M. T. Montgomery (2008), Observed structure, evolution, and potential intensity of category 5 Hurricane Isabel (2003) from 12 to 14 September, *Mon. Weather Rev.*, *136*, 2023–2046.
Bui, H. H., R. K. Smith, M. T. Montgomery, and J. Peng (2009), Balanced and unbalanced aspects of tropical cyclone intensification, *Q. J. R. Meteorol. Soc.*, *135*, 1715–1731.
Cotton, W. R., et al. (2003), RAMS 2001: Current status and future directions, *Meteorol. Atmos. Phys.*, *82*, 5–29.
Cram, T. A., J. Persing, M. T. Montgomery, and S. A. Braun (2007), A Lagrangian trajectory view on transport and mixing processes between the eye, eyewall, and environment using a high-resolution simulation of Hurricane Bonnie (1998), *J. Atmos. Sci.*, *64*, 1835–1856.
Davis, C., et al. (2008), Prediction of landfalling hurricanes with the Advanced Hurricane WRF Model, *Mon. Weather Rev.*, *136*, 1990–2005.
Eliassen, A. (1971), On the Ekman layer in a circular vortex, *J. Meteorol. Soc. Jpn.*, *49*, 784–789.
Eliassen, A., and M. Lystad (1977), The Ekman layer of a circular vortex: A numerical and theoretical study, *Geophys. Norv.*, *31*, 1–16.
Gill, A. (1982), *Atmosphere-Ocean Dynamics*, Academic, San Diego, Calif.
Harrington, J. Y. (1997), *The effects of radiative and microphysical processes on simulated warm and transition season Arctic stratus*, PhD thesis, 289 pp., Colo. State Univ., Fort Collins.
Hill, G. E. (1974), Factors controlling the size and spacing of cumulus clouds as revealed by numerical experiments, *J. Atmos. Sci.*, *31*, 646–673.
Holton, J. R. (2004), *An Introduction to Dynamic Meteorology*, 535 pp., Elsevier.
Jordan, C. L. (1958), Mean soundings for the West Indies area, *J. Meteorol.*, *15*, 91–97.
Kepert, J. (2001), The dynamics of boundary layer jets within the tropical cyclone core. Part I: Linear theory, *J. Atmos. Sci.*, *58*, 2469–2484.
Kepert, J., and Y. Wang (2001), The dynamics of boundary layer jets within the tropical cyclone core. Part II: Nonlinear enhancement, *J. Atmos. Sci.*, *58*, 2485–2501.
Kepert, J. D. (2006), Observed boundary layer wind structure and balance in the hurricane core. Part I: Hurricane Georges, *J. Atmos. Sci.*, *63*, 2169–2193, doi:10.1175/JAS3745.1.
Kepert, J. D. (2012), Choosing a boundary layer parameterization for tropical cyclone modeling, *Mon. Weather Rev.*, *140*, 1427–1445.
Kepert, J. D. (2013), How does the boundary layer contribute to eyewall replacement cycles in axisymmetric tropical cyclones?, *J. Atmos. Sci.*, *70*, 2808–2830.
Kepert, J. D., and D. S. Nolan (2014), Reply to "Comments on 'How does the boundary layer contribute to eyewall replacement cycles in axisymmetric tropical cyclones?,'" *J. Atmos. Sci.*, *71*, 4692–4704.
Lilly, D. K. (1962), On the numerical simulation of buoyant convection, *Tellus*, *14*, 148–172.
Louis, J.-F. (1979), A parametric model of vertical eddy fluxes in the atmosphere, *Boundary Layer Meteorol.*, *17*, 187–202.
Marks, F. D., P. Black, M. T. Montgomery, and R. W. Burpee (2008), Structure of the eye and the eyewall of Hurricane Hugo (1989), *Mon. Weather Rev.*, *136*, 1237–1259.
McWilliams, J. C. (1971), *The boundary layer dynamics of symmetric vortices*, PhD thesis, 89 pp., Harvard Univ. Press, Ann Arbor, Mich.
McWilliams, J. C. (2011), *Fundamentals of Geophysical Fluid Dynamics*, 249 pp., Cambridge Univ. Press, Cambridge, U. K.
Montgomery, M. T., M. E. Nicholls, T. A. Cram, and A. B. Saunders (2006a), A vortical hot tower route to tropical cyclogenesis, *J. Atmos. Sci.*, *63*, 355–386.
Montgomery, M. T., M. M. Bell, S. D. Aberson, and M. L. Black (2006b), Hurricane Isabel (2003): New insights into the physics of intense storms. Part I: Mean vortex structure and maximum intensity estimates, *Bull. Am. Meteorol. Soc.*, *87*, 1335–1347.
Montgomery, M. T., S. F. Abarca, R. K. Smith, C.-C. Wu, and Y.-H. Huang (2014a), Comments on "How does the boundary layer contribute to eyewall replacement cycles in axisymmetric tropical cyclones?," *J. Atmos. Sci.*, *71*, 4682–4691.
Montgomery, M. T., J. A. Zhang, and R. K. Smith (2014b), An analysis of the observed low-level structure of rapidly intensifying and mature hurricane Earl (2010), *Q. J. R. Meteorol. Soc.*, *140*, 2132–2146.
Persing, J., M. T. Montgomery, J. C. McWilliams, and R. K. Smith (2013), Asymmetric and axisymmetric dynamics of tropical cyclones, *Atmos. Chem. Phys.*, *13*, 12,299–12,341.
Pielke, R. A., et al. (1992), A comprehensive meteorological modeling system-RAMS, *Meteorol. Atmos. Phys.*, *49*, 69–91.
Rotunno, R., and K. A. Emanuel (1987), An air-sea interaction theory for tropical cyclones. Part II: Evolutionary study using a nonhydrostatic axisymmetric numerical model, *J. Atmos. Sci.*, *44*, 542–561.
Sanger, N. T., M. T. Montgomery, R. K. Smith, and M. M. Bell (2014), An observational study of tropical cyclone spinup in Supertyphoon Jangmi (2008) from 24 to 27 September, *Mon. Weather Rev.*, *142*, 3–28.
Slocum, C. J., G. J. Williams, R. K. Taft, and W. H. Schubert (2014), Tropical cyclone boundary layer shocks, paper presented at NCAR/NOAA/CSU Tropical Cyclone Workshop, Boulder, Colo.
Smagorinsky, J. (1963), General circulation experiments with the primitive equations. Part I: The basic experiment, *Mon. Weather Rev.*, *91*, 99–164.
Smith, R. K. (1968), The surface boundary layer of a hurricane, *Tellus*, *20*, 473–484.
Smith, R. K., and M. T. Montgomery (2010), Hurricane boundary-layer theory, *Q. J. R. Meteorol. Soc.*, *136*, 1665–1670.
Smith, R. K., M. T. Montgomery, and V. S. Nguyen (2009), Tropical cyclone spin-up revisited, *Q. J. R. Meteorol. Soc.*, *135*, 1321–1335.
Stern, D. P., J. L. Vigh, D. S. Nolan, and F. Zhang (2015), Revisiting the relationship between eyewall contraction and intensification, *J. Atmos. Sci.*, *72*, 1283–1306.
Terwey, W., S. F. Abarca, and M. T. Montgomery (2013), Comments on "Convectively generated potential vorticity in rainbands and formation of the secondary eyewall in Hurricane Rita of 2005," *J. Atmos. Sci.*, *70*, 984–988.

Terwey, W. D., and M. T. Montgomery (2008), Secondary eyewall formation in two idealized, full-physics modeled hurricanes, *J. Geophys. Res.*, *113*, D12112, doi:10.1029/2007JD008897.

Vogl, S., and R. K. Smith (2009), Limitations of a linear model for the hurricane boundary layer, *Q. J. R. Meteorol. Soc.*, *135*, 839–850.

Walko, R. L., W. R. Cotton, M. P. Myers, and J. Y. Harrington (1995), New RAMS cloud microphysics parameterization. Part I: The single-moment scheme, *Atmos. Res.*, *38*, 29–62.

Whitham, G. B. (1974), *Linear and Nonlinear Waves*, 636 pp., John Wiley.

Williams, G. J. (2015), The effects of vortex structure and vortex translation on the tropical cyclone boundary layer wind field, *J. Adv. Model. Earth Syst.*, *7*, 188–214, doi:10.1002/2013MS000299.

Williams, G. J., R. K. Taft, B. D. McNoldy and W. H. Schubert (2013), Shock-like structures in the tropical cyclone boundary layer, *J. Adv. Model. Earth Syst.*, *5*, 338–353, doi:10.1002/jame.20028.

Zhang, J. A., F. D. Marks, M. T. Montgomery, and S. Lorsolo (2011), An estimation of turbulent characteristics in the low-level region of intense Hurricanes Allen (1980) and Hugo (1989), *Mon. Weather Rev.*, *139*, 1447–1462.